Journal of Molecular Structure 1242 (2021) 130815

Contents lists available at ScienceDirect

Journal of Molecular Structure

journal homepage: www.elsevier.com/locate/molstr

Nickel(II) Complexes with Polyhydroxybenzaldehyde and O,N,S tridentate Thiosemicarbazone ligands: Synthesis, Cytotoxicity, Antimalarial Activity, and Molecular Docking Studies.

Savina Savir[a], Jonathan Wee Kent Liew[b], Indra Vythilingam[b], Yvonne Ai Lian Lim[b], Chun Hoe Tan[c], Kae Shin Sim[c], Vannajan Sanghiran Lee[a], Mohd. Jamil Maah[a], Kong Wai Tan[a,*]

[a] Department of Chemistry, Faculty of Science, University of Malaya, 50603 Kuala Lumpur, Malaysia
[b] Department of Parasitology, Faculty of Medicine, University of Malaya, 50603 Kuala Lumpur, Malaysia
[c] Institute of Biological Sciences, Faculty of Science, University of Malaya, 50603 Kuala Lumpur, Malaysia

ARTICLE INFO

Article history:
Received 10 January 2021
Revised 21 May 2021
Accepted 30 May 2021
Available online 3 June 2021

Keywords:
Thiosemicarbazone
Triphenylphosphine
Cytotoxic activity
Antimalarial activity
Molecular docking

ABSTRACT

A series of Schiff base metal complexes with the formulations [Ni(**L1**)PPh_3]Cl (**1**), [Ni(**L2**)PPh_3]Cl (**2**), [Ni(**L3**)PPh_3] (**3**), and [Ni(**L4**)PPh_3] (**4**) (where **L1** = 2,3,4-trihydroxybenzaldehyde-4-methyl-3-thiosemicarbazone, **L2** = 2,3,4-trihydroxybenzaldehyde-4-ethyl-3-thiosemicarbazone, **L3** = 2,3,4-trihydroxybenzaldehyde-4-phenyl-3-thiosemicarbazone, and **L4** = 2,3,4-trihydroxybenzaldehyde-4-(4-ethylphenyl)-3-thiosemicarbazone) were synthesised. All compounds were characterised using FT-IR, ^{1}H NMR, and ^{13}C NMR. The complexes were further characterised with single crystal X-ray diffraction. The complexes are four-coordinated and adopt a square planar geometry, in which the Schiff base ligands bind to the metal centre *via* their tridentate O,N,S atoms. Ligand **L2** and complex **1** showed a higher cytotoxic activity than cisplatin with IC_{50} 5.75 ± 0.49 and 4.26 ± 0.29 μM, respectively when tested against human colorectal carcinoma HCT 116. Besides, complex **3** was found to show a stronger cytotoxic activity with an IC_{50} 7.07 ± 0.61 μM than its ligand (**L3** IC_{50} 9.82 ± 1.85 μM) when tested against HCT 116. On the other hand, complexes **2** and **3** showed moderate in vitro antimalarial activity with IC_{50} 9.88 ± 0.23 and 1.06 ± 0.01 μM, respectively. Remarkably, the antimalarial activity increases as the hydrophobicity of the substituent group attached at the N(3) position increases. Through molecular docking simulation, complexes **2** and **3** are predicted to be a minor groove binder with an appreciable DNA binding affinity, suggesting that **2** and **3** exerted their cytotoxicity and antiplasmodial activity probably *via* their benzaldehyde, triphenylphosphine, aliphatic chain and phenyl moieties interaction with DNA base pairs.

1. Introduction

The global cancer burden is approximated to have increased to 18.1 million new cases and 9.6 million deaths in 2018 [1]. Since the discovery of cisplatin in 1965 for cancer treatment, the development of platinum-based drugs in the field of research have become compellingly in demand [2]. The other platinum compounds that had entered clinical trials as anticancer agents years ago were carboplatin, oxaliplatin, and nedaplatin [3]. Approval of cisplatin for clinical use has led to more constructive treatments against testicular, ovarian, cervical, bladder, head and neck, and small-cell lung cancers [4]. Cisplatin induces apoptosis in cancer cells by forming crosslinks with the purine bases on the DNA and interfering with DNA's repair mechanism [5]. However, the efficacy of platinum drugs are greatly restricted by severe side effects due to poor specificity, drug resistance, and systemic toxicities such as nephrotoxicity, neurotoxicity, ototoxicity, and emetogenesis [6]. Hence, new anticancer drugs have to be constantly synthesised to address the issues caused by the existing drugs. Previous studies have shown that pyrimethamine which is an antimalarial drug, is able to induce apoptosis of cancer cells, acting as an antitumor drug simultaneously [7]. Thus, it would be enthraling if the compounds studied in this paper could have cytotoxic activity and act as antimalarial drugs at the same time.

Malaria is a vector-borne endemic contagious ailment that is brought about by parasitic protozoa of the genus *Plasmodium*. The four significant species that cause malaria in humans are the *P.*

* Corresponding author.
E-mail address: kongwai@um.edu.my (K.W. Tan).

https://doi.org/10.1016/j.molstruc.2021.130815
0022-2860/

falciparum, P. vivax, P. ovale, and *P. malariae*. The severe form, however, is caused by the former [8]. According to the World Malaria report 2019, 228 million cases of the disease and 405,000 of global malaria deaths were reported in 2018, while most of the reported mortality are amongst the young children (a child dies of malaria in every two minutes) [9]. Factually, chloroquine (CQ), a 4-aminoquinoline drug, has been the most established antimalarial drug due to its satisfactory potency, low toxicity, and low cost [10]. However, the *P. falciparum* has become resistant to CQ [11,12], along with other antimalarial drugs such as sulfadoxine–pyrimethamine (SU-PY), mefloquine (MQ), and artemisinin. Hence, discoveries of chloroquine followed by artemisinin were able to ward off malarial infection for some time until the parasite acquired resistance towards these drugs. Soon after, the therapeutic potential of ferroquine (FQ), which was once considered the most potent organometallic antimalarial drug was explored. FQ was found to be exceedingly active in vitro against both CQ-resistant and CQ-susceptible *P. falciparum* and *P. vivax* isolates from different endemic areas [13,14]. Unfortunately, treatment with FQ was found to result in gastrointestinal side effects and central nervous disorders [15]. Hence, the discoveries of new drugs are crucial to address the issue of resistance and adverse effects.

Thiosemicarbazones (TSC) have a wide range of pharmacological and biological properties, including antitumor and antimalarial. These properties are dependant upon the chemical nature of the moiety attached to the $C = S$ carbon atom in TSC [16]. Mostly, metal complexation by anionic ligands that resulted in charge neutral metal complexes were found to exhibit improved bioactivity than the neutral ligands because the negative charge of the sulfur atom enhances the coordination strength [17,18]. In this case, the thiol tautomer was seen to show better cytotoxicity and improved antimalarial activity than its original thione form. Their coordinating ability as chelate ligands has enabled them to be used for the synthesis of a vast range of complexes. They have been studied thoroughly as ligands to form complexes with different transition metals due to the presence of their electron donating functional groups, which is their O,N,S tridentate binding sites [19]. Many studies have demonstrated that even slight structure modifications may result in dramatic chemical and biological changes in metal thiosemicarbazone complex [20]. Hence, the properties of TSC have made them adaptable to an extensive array of applications, making them appealing for further analysis as potential therapeutic agents aimed at malaria and cancer treatments.

Triphenylphosphine (TPP) is used as secondary ligand in this study because phosphine based compounds have widespread pharmacological applications such as antiviral, antioxidant, antifungal, anticarcinogenic, antitumor, and antibacterial by nature [21]. Explicitly, phosphine based nickel(II) and palladium(II) complexes have been reported to possess significant bioactivities [22]. In cancer treatment, TPP, which is a mitochodriotropic ligand is expected to transfer the metal ion into the cancer cells [23]. Besides, TPP is used in the metal complexation process because it acts as a catalyst in the synthesis of organic and inorganic compounds to speed up the rate of a chemical reaction [24]. An important factor that influences the antimalarial activity of a compound is its hydrophobicity. The higher the hydrophobicity, the more potent its activity [25,26]. Hence, the hydrophobic aromatic rings in TPP may accentuate the antimalarial activity of the synthesised compounds.

We are enthusiastic in developing nickel complexes of thiosemicarbazone because they have been reported to have high cytotoxic activity. Nickel(II) complexes were shown as telomerase and topoisomerase II inhibitors that induce cancer cell apoptosis *via* mitochondrial pathways [27]. In addition, metal complexes are believed to exhibit cytotoxic and antimalarial activities better than their free ligands as the latter may show little or no activities at all [28]. Hence, metal chelating abilities account for the cytotoxic and antimalarial activities of a metal complex. Besides, complexation of transition metals with compounds having antimalarial activity further enhances the pharmacological and chemical properties such as potency, selectivity, chemical stability, and lipophilicity of the compound [29]. Having mentioned that, the lipophilic nature of the metal helps with the cellular uptake process of the parasite as it aids in the transportation of the metal-free thiosemicarbazones into cellular components. In a nutshell, metal chelators can deprive parasites from metal ions crucial for their survival and utilize the newly formed metal-chelator hybrid (complex) to induce oxidative insult to the parasites.

Previous research on polyhydroxybenzaldehyde thiosemicarbazone derivatives suggested that complexes of nickel where the ligand was coordinated to the metal centre *via* its tridentate O,N,S atom was effective towards several cancer cell lines [30]. Although some ligands of the 2,3,4-trihydroxybenzaldehyde derivatives have been synthesised and reported [31,32], further characterisation and biological studies of their metal complexes still warrant further investigations. Previously, we reported the synthesis, cytotoxicity, and antimalarial activity of nickel(II) complexes with Schiff base ligands derived from fluorene-2-carboxaldehyde and thiosemicarbazide [33]. In the present, we focus on the synthesis of nickel (II) complex and triphenylphosphine with Schiff base ligands derived from polyhydroxybenzaldehydes and thiosemicarbazides. Their cytotoxicity, antimalarial activity, and DNA binding affinity were also reported.

2. Experimental

2.1. Materials and solutions

The chemicals for synthesis (thiosemicarbazides, 2,3,4-trihydroxybenzaldehyde, nickel(II)chloride hexahydrate, triphenylphosphine, and chloroquine phosphate) were purchased from Sigma Aldrich, Germany and Alfa Aesar, England. Solvents were purchased from Merck, Germany.

2.2. Physical measurements

Perkin-Elmer Spectrum RX-1 spectrometer was used to record the FT-IR spectra of all the ligands and metal complexes. They were recorded as KBr pellets. The NMR spectra was determined in a DMSO–d_6 with a JEOL ECX 400 spectrometer at 400 MHz. The percentage of carbon, hydrogen and nitrogen was determined using A Thermo Finnigan Eager 300 CHN elemental analyser. Any crystals collected as a result of recrystallisation were subjected to X-RAY using a Rigaku Oxford (formerly Agilent Technologies) Super Nova Dual diffractometer with Cu Kα (λ = 1.541 84 Å) radiation at 160−170 K.

2.3. Syntheses

- *Synthesis of 2,3,4-trihydroxybenzaldehyde-4-methyl-3-thiosemicarbazone (**L1**)*

The ligand was prepared by following a published procedure with slight changes [31]. The ethanolic solution containing 2,3,4-trihydroxybenzaldehyde and 4-methyl-3-thiosemicarbazide was refluxed for 4 h. The brown powder formed from cooled solution was recrystallized with ethanol. Yield: 0.27 g, 81%. Anal. Calc. for $C_9H_{11}N_3O_3S$: C, 44.80; H, 4.60; N, 17.42. Found: C, 44.13; H, 4.45; N, 16.86%. IR (KBr disc, cm^{-1}): 3452 s, 3202 w, 3180 m, 1637s, 1346 w, 1283s, 823 s (s, strong; m, medium; w, weak). ^1H NMR signals (DMSO–d_6, TMS, ppm): 11.19 (s, 1H, N(2)H), 9.53 (s, 1H, OH), 8.96 (s, 1H, OH), 8.41 (s, 1H, N(3)H), 8.23 (d, 1H, OH, J = *4.58 Hz*), 8.19 (s, 1H, CH=*N*), 7.12 (d, 1H, aromatic, J = *8.70 Hz*),

6.32 (d, 1H, aromatic, *J = 8.70 Hz*), 2.95 (d, 3H, CH_3, *J = 4.58 Hz*). ^{13}C NMR signals (DMSO–d_6, TMS, ppm): 177.51 (*C = S*), 141.87 (*C = N*), 148.62 (C–OH), 146.99 (C–OH), 133.20 (C–OH), 118.45, 113.15, 108.43 (C-aromatic), 31.33 (CH_3).

2.4. Melting point: 110–114 °C

- *Synthesis of 2,3,4-trihydroxybenzaldehyde-4-ethyl-3-thiosemi carbazone (**L2**)*

Similar to the preparation of (**L1**) by using 4-ethyl-3-thiosemicarbazide. Yield: 0.31 g, 91%. Anal. Calc. for $C_{10}H_{15}N_3O_4S$: C, 43.95; H, 5.53; N, 15.37. Found: C, 44.58; H, 5.32; N, 15.50%. IR (KBr disc, cm^{-1}): 3439 s, 3349 w, 3170 m, 1632s, 1348 w, 1251s, 798 m (s, strong; m, medium; w, weak). ^{1}H NMR signals (DMSO–d_6, TMS, ppm): 11. 12 (s, 1H, N(2)H), 9.53 (s, 1H, OH), 8.99 (s, 1H, OH), 8.43 (s, 1H, OH), 8.26 (t, 1H, N(3)H, *J = 11.45 Hz*), 8.19 (s, 1H, CH=*N*), 7.11 (d, 1H, aromatic, *J = 8.24 Hz*), 6.32 (d, 1H, aromatic, *J = 8.70 Hz*), 3.53 (q, 2H, CH_2, *J = 20.61 Hz*), 1.08 (t, 3H, CH_3, *J = 14.20 Hz*) . ^{13}C NMR signals (DMSO–d_6, TMS, ppm): 176.44 (*C = S*), 142.01 (*C = N*), 148.64 (C–OH), 146.96 (C–OH), 133.20 (C–OH), 118.55, 113.10, 108.16 (C-aromatic), 38.76 (CH_2), 15.23 (CH_3).

2.5. Melting point: 108–110 °C

- *Synthesis of 2,3,4-trihydroxybenzaldehyde-4-phenyl-3-thiosemi carbazone (**L3**)*

Similar to the preparation of (**L1**) by using 4-phenyl-3-thiosemicarbazide. Yield: 0.29 g, 89%. Anal. Calc. for $C_{14}H_{13}N_3O_3S$: C, 55.43; H, 4.32; N, 13.85. Found: C, 55.34; H, 3.79; N, 13.67%. IR (KBr disc, cm^{-1}): 3531, 3441 s, 3149 w, 1612s, 1345 w, 1261s, 804 m (s, strong; m, medium; w, weak). ^{1}H NMR signals (DMSO–d_6, TMS, ppm): 11. 56 (s, 1H, N(2)H), 9.89 (s, 1H, OH), 9.58 (s, 1H, OH), 8.46 (s, 1H, N(3)H), 8.31 (s, 1H, CH=*N*), 6.34 (d, 1H, OH, *J = 8.70 Hz*), 7.54 (d, 2H, aromatic, *J = 7.79 Hz*), 7.31 (t, 3H, aromatic, *J = 15.57 Hz*), 7.13 (t, 2H, aromatic, *J = 14.65 Hz*). ^{13}C NMR signals (DMSO–d_6, TMS, ppm): 175.54 (*C = S*), 147.19 (*C = N*), 153.76 (C–OH), 151.42 (C–OH), 148.90 (C–OH), 142.80, 139.68, 133.19, 129.59, 128.50, 125.80, 125.45, 118.93, 112.93, 108.19 (C-aromatic).

2.6. Melting point: 124–128 °C

- *Synthesis of 2,3,4-trihydroxybenzaldehyde-4-(4-ethylphenyl)−3-thiosemicarbazone (**L4**)*

Similar to the preparation of (**L1**) by using 4-(4-ethylphenyl)−3-thiosemicarbazide. Yield: 0.25 g, 81%. Anal. Calc. for $C_{16}H_{17}N_3O_3S$: C, 57.99; H, 5.17; N, 12.68. Found: C, 57.52; H, 4.98; N, 12.25%. IR (KBr disc, cm^{-1}): 3352, 3341, 3140 s, 1634s, 1378 w, 1271s, 833 m (s, strong; m, medium; w, weak). ^{1}H NMR signals (DMSO–d_6, TMS, ppm): 11. 51 (s, 1H, N(2)H), 9.84 (d, 1H, OH, *J = 16.72 Hz*), 9.65 (s, 1H, N(3)H), 8.33 (s, 1H, CH=*N*), 6.49 (d, 1H, OH, *J = 8.24 Hz*), 6.37 (d, 1H, OH, *J = 8.70 Hz*), 7.44 (d, 2H, aromatic, *J = 8.24 Hz*), 7.18 (d, 2H, aromatic, *J = 8.24 Hz*), 7.10 (d, 2H, aromatic, *J = 8.24 Hz*), 2.59 (q, 2H, CH_2, *J = 22.90 Hz*), 1.17 (t, 3H, CH_3, *J = 15.11 Hz*). ^{13}C NMR signals (DMSO–d_6, TMS, ppm): 175.59 (*C = S*), 147.16 (*C = N*), 153.76 (C–OH), 151.42 (C–OH), 148.85 (C–OH), 140.99, 137.30, 132.68, 127.78, 125.85, 118.90, 115.91, 112.95, 108.18 (C-aromatic).

2.7. Melting point: 104–108 °C

- *Synthesis of (2,3,4-trihydroxybenzaldehyde-4-methyl-3-thiosemi carbazonato)-(triphenylphosphine)Ni(II)* [Ni(**L1**)PPh_3]Cl, *(**1**)*

The ethanolic solution containing the ligand (**L1**), triphenylphosphine and nickel(II)chloride hexahydrate was refluxed for 6 h. The solution was left aside for slow evaporation. Brown precipitate formed was then recrystallized with either ethanol or a mixture of DMF and acetonitrile in a 1:2 ratio to promote crystal growth. Yield: 0.18 g, 63%. Anal. Calc. for $C_{27}H_{25}ClN_3NiO_3PS.H_2O$: C, 54.35; H, 4.22; N, 7.04. Found: C, 54.99; H, 4.74; N, 6.63%. IR (KBr disc, cm^{-1}): 3427, 3310 s, 3169 m, 1616s, 1434s, 1380 m, 1273s, 1084s, 788 m, 689 s, 533 m, 509 s, 488 m (s, strong; m, medium; w, weak). ^{1}H NMR signals (DMSO–d_6, TMS, ppm): 11. 17 (s, 1H, N(2)H), 8.23 (s, 1H, N(3)H), 8.19 (s, 1H, CH=*N*), 6.44 (d, 1H, OH, *J = 8.24 Hz*), 6.32 (d, 1H, OH, *J = 8. 24 Hz*), 7.58 (d, 3H, aromatic, *J = 7.33 Hz*), 7.39 (s, 12H, aromatic), 7.12 (d, 1H, aromatic, *J = 8.24 Hz*), 7.04 (d, 1H, aromatic, *J = 8.24 Hz*), 2.93 (d, 3H, CH_3, *J = 3.66 Hz*). ^{13}C NMR signals (DMSO–d_6, TMS, ppm): 177.29 (*C = S*), 141.65 (*C = N*), 148.59 (C–OH), 146.91 (C–OH), 134.08 (C–O-Ni), 133.15, 130.73, 129.33, 118.26, 112.93, 108.26 (C-aromatic).

2.8. Melting point: 180–184 °C

- *Synthesis of (2,3,4-trihydroxybenzaldehyde-4-ethyl-3-thiosemi carbazonato)-(triphenylphosphine)Ni(II)* [Ni(**L2**)PPh_3]Cl, *(**2**)*

Similar to the preparation of (**1**) by using ligand (**L2**). Yield: 0.22 g, 71%. Anal. Calc. for $C_{28}H_{26}ClN_3NiO_3PS.H_2O$: C, 55.07; H, 4.46; N, 6.88. Found: C, 55.41; H, 5.06; N, 6.23%. IR (KBr disc, cm^{-1}): 3454, 3218 s, 3161 s, 1610s, 1435s, 1320 m, 1292s, 1091s, 779 m, 691 s, 528 m, 503 s, 494 m (s, strong; m, medium; w, weak). ^{1}H NMR signals (DMSO–d_6, TMS, ppm): 11. 10 (s, 1H, N(2)H), 8.27 (s, 1H, N(3)H), 8.18 (s, 1H, CH=*N*), 6.33 (d, 1H, OH, *J = 8.24 Hz*), 6.05 (s, 1H, OH), 7.42 (s, 16H, aromatic), 7.11 (d, 1H, aromatic, *J = 8.70 Hz*), 1.27 (s, 2H, CH_2), 1.06 (t, 3H, CH_3, *J = 13.74 Hz*). ^{13}C NMR signals (DMSO–d_6, TMS, ppm): 176.35 (*C = S*), 141.45 (*C = N*), 148.60 (C–OH), 146.91 (C–OH), 134.04 (C–O-Ni), 133.14, 132.59, 132.22, 132.12, 131.99, 131.91, 129.32, 118.03, 113.12, 108.23 (C-aromatic), 38.78 (CH_2), 15.22 (CH_3).

2.9. Melting point: 140–144 °C

- *Synthesis of (2,3,4-trihydroxybenzaldehyde-4-phenyl-3-thiosemi carbazonato)-(triphenylphosphine)Ni(II) [Ni(**L3**)PPh3], (**3**)*

Similar to the preparation of (**1**) by using ligand (**L3**). Yield: 0.22 g, 71%. Anal. Calc. for $C_{32}H_{27}N_3NiO_3PS$: C, 61.66; H, 4.37; N, 6.74. Found: C, 61.35; H, 5.08; N, 6.41%. IR (KBr disc, cm^{-1}): 3448, 3370, 1562s, 1436s, 1318 m, 1239s, 1093s, 765 s, 690 s, 529 m, 507 s, 489 m (s, strong; m, medium; w, weak). ^{1}H NMR signals (DMSO–d_6, TMS, ppm): 9.25 (s, 1H, N(3)H), 9. 25 (s, 1H, OH), 8.45 (d, 1H, CH=*N, J = 8.70 Hz*), 7.76 (t, 6H, aromatic, *J = 17.86 Hz*), 7.62 (d, 3H, aromatic, *J = 8.24 Hz*), 7.54 (t, 9H, aromatic, *J = 13.28 Hz*), 7.18 (t, 2H, aromatic, *J = 15.57 Hz*), 6.85 (t, 2H, aromatic, *J = 16.03 Hz*), 6.21 (d, 1H, OH, *J = 8.70 Hz*), 4.70 (s, 1H, SH). ^{13}C NMR signals (DMSO–d_6, TMS, ppm): 164.87 (*C = N*), 164.70 (*C = N*), 153.42 (C–O-Ni), 150.25 (C–OH), 146.48 (C–OH), 141.92, 134.43, 134.33, 133.70, 131.83, 129.55, 129.45, 128.97, 123.26, 121.51, 118.44, 110.79, 107.86 (C-aromatic).

2.10. Melting point: 264–268 °C

- *Synthesis of (2,3,4-trihydroxybenzaldehyde-4-(4-ethylphenyl)−3-thiosemicarbazonato)-(triphenylphophine)Ni(II) [Ni(**L4**)PPh3], (**4**)*

Similar to the preparation of (**1**) by using ligand (**L4**). Yield: 0.22 g, 71%. Anal. Calc. for $C_{37}H_{43}N_4NiO_7PS$: C, 58.44; H, 5.57; N, 7.37. Found: C, 58.98; H, 5.57; N, 7.83%. IR (KBr disc, cm^{-1}): 3441, 3296, 3187, 1654s, 1436s, 1315 m, 1277s, 1095s, 782 s,

693, 531 m, 510 s, 493 m (s, strong; m, medium; w, weak). ^{1}H NMR signals (DMSO–d_6, TMS, ppm): 9.21 (s, 1H, OH), 9.14 (s, 1H, N(3)H), 8.40 (d, 1H, CH=*N, J = 8.70 Hz*), 7.74 (t, 6H, aromatic, *J = 17.86 Hz*), 7.52 (t, 9H, aromatic, *J = 18.72 Hz*), 7.01 (d, 4H, aromatic, *J = 8.70 Hz*), 6.82 (d, 2H, aromatic, *J = 8.70 Hz*), 6.17 (d, 1H, OH, *J = 8.70 Hz*), 4.68 (s, 1H, SH), 2.45 (q, 2H, CH_2, *J = 5.50 Hz*), 1.08 (t, 3H, CH_3, *J = 15.11 Hz*). ^{13}C NMR signals (DMSO–d_6, TMS, ppm): 164.84 (*C = N*), 164.67 (*C = N*), 153.06 (C–O-Ni), 150.16 (C–OH), 146.39 (C–OH), 139.75, 136.88, 134.43, 134.33, 132.06, 131.96, 131.82, 129.54, 129.44, 129.01, 128.16, 123.18, 118.63, 110.83, 107.81 (C-aromatic), 28.04 (CH_2), 16.38 (CH_3).

2.11. Melting point: 156–160 °C

2.11.1. X-ray crystallography

In this research, all complexes were recrystallised from dimethylformamide (DMF). The complexes are all dark brown in colour. A Rigaku Oxford (formerly Agilent Technologies) Super Nova Dual diffractometer with Cu Kα (λ = 1.541 84 Å) radiation at 160−170 K was used to generate the unit cell parameter and intensity data. OLEX2 was used to label atoms [34]. The structure was solved with the SHELXS structure solution program using Direct Methods and refined with the SHELXL refinement package using Least Squares minimisation [35]. All non-hydrogen atoms were refined anisotropically and hydrogen atoms were added at calculated position and refined as a riding model. Whereas, the crystal structure visualisation and analysis were done using Mercury CSD 2.0 [36]. In addition, the publCIF software was used to edit, validate and format crystallographic information files [37].

2.12. Biological assays

2.12.1. Cell culture and MTT cytotoxicity assay

The assay was performed as previously described [45] using human colorectal carcinoma HCT 116, prostate adenocarcinoma PC-3, and breast adenocarcinoma MCF7 cell lines which were purchased from American Type Culture Collection (ATCC, USA). The IC_{50} values were determined by plotting percentage of viability against the concentration of treatment on a logarithmic scale using GraphPad Prism 7 software (Graphpad software Inc., CA, USA).

2.12.2. Determination of antimalarial activity by testing on plasmodium falciparum culture

This experiment was conducted by using the *P. falciparum* 3D7 strain, according to our previously published procedures [33]. The drug plates containing culture medium and blood media parasite mixture (BMPM) were incubated in a gas chamber containing 5% CO_2, 5% O_2, and 90% N_2 at 37.5–38.0 °C for 36 to 42 h until at least 50% of the ring stage parasites had matured to schizonts [38]. Thick blood smears were made for each concentration from the erythrocytes that remained in the fluid once the supernatants were removed. After thorough drying, they were stained with 10% Giemsa stain [39]. Microscopic evaluation was done by counting the number of schizonts with five or more nuclei out of a total 200 asexual parasites in every thick film. [40]. Results were reported as mean (±SD) of two different experiments which were performed in duplicates each. IC_{50} values were generated using GraphPad Prism 7 software (Graphpad software Inc., CA, USA).

2.13. Molecular docking studies

The AutoDock Vina 1.12 [41] software was used to perform theoretical computational docking calculations for the interaction of complexes **1, 2**, and **3** with DNA structures extracted from Protein Data Bank (PDB) with PDB entry 1BNA [42] and 1XRW [43]. DNA and complexes **1, 2** and **3** were minimised using AMBER force field and AMI-BCC charges where the solvents and a dual metalating/intercalating DNA binding drug in 1XRW were removed from the Xray structures. The non-polar hydrogens of the complexes were merged. In addition, the autodocktools (ADT) was used to set ligand to be flexible and perform the docking to the rigid DNA structures. The binding affinities of docked compounds were estimated using docking area of a grid box 25 × 25 × 25 with grid spacing of 0.375 Å. The aforementioned dimensions of docking area were adequate to include the entire DNA molecule, ensuring that the space for free rotation of ligand and fitting of the receptor is sufficient. The simulations obtained from the docking experiment were positioned in order of increasing energy and clustered in a group of similar conformation. Optimal binding mode was determined by the pose with the least energy. The UCSF Chimera 1.14 software was used to visualise the 3D images of docked conformation [44].

3. Results and discussion

3.1. Synthesis of ligands and metal complexes

The proposed structures of all compounds and their method of synthesis is shown in Fig. 1 and Scheme 1, respectively. All ligands and complexes were obtained in good yield with sharp melting points. Besides, the proposed structures were in good agreement with the data obtained from various spectroscopic analysis. Results from elemental analyses for all compounds corroborated with the proposed formulation from crystal data. The ligands (**L1-L4**) were yellowish brown in colour and the complexes (**1–4**) were blackish brown in colour. Ligands (**L1-L2**) were found to be coordinating to the metal centre in the thione form whereas ligands (**L3-L4**) were found to be coordinating to the metal centre in the thiolate form. Besides, all ligands and complexes are soluble in selected polar solvents such as ethanol, methanol, DMF and DMSO. To the best of our knowledge, spectroscopic data of ligands **L1, L2, L3** and **L4** are consistent with similar compounds that were previously reported [32,45].

3.2. Infrared spectra

3.2.1. Infrared spectra of ligands (*L1-L4*)

Table 1 shows the infrared spectra of ligands and complexes. All ligands have the azomethine imine peak at a range of 1612–1637 cm^{-1} [46]. The thioamide *ν*(NC=*S*) peaks for all ligands

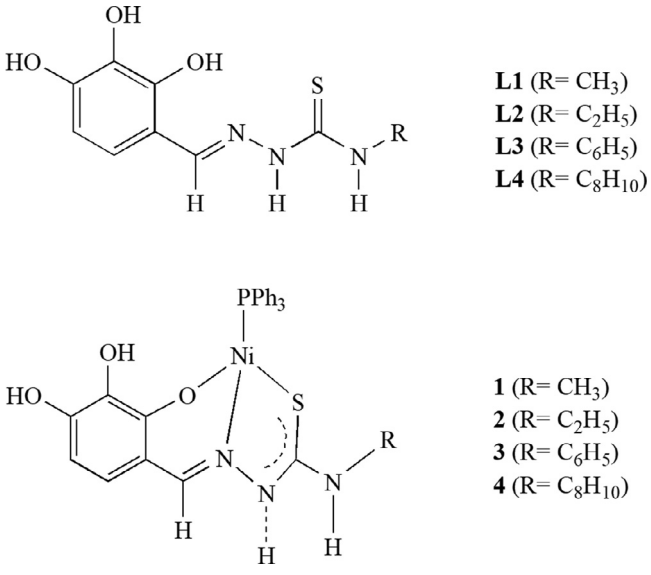

Fig. 1. Proposed structures of ligands (**L1-L4**) and complexes (**1–4**).

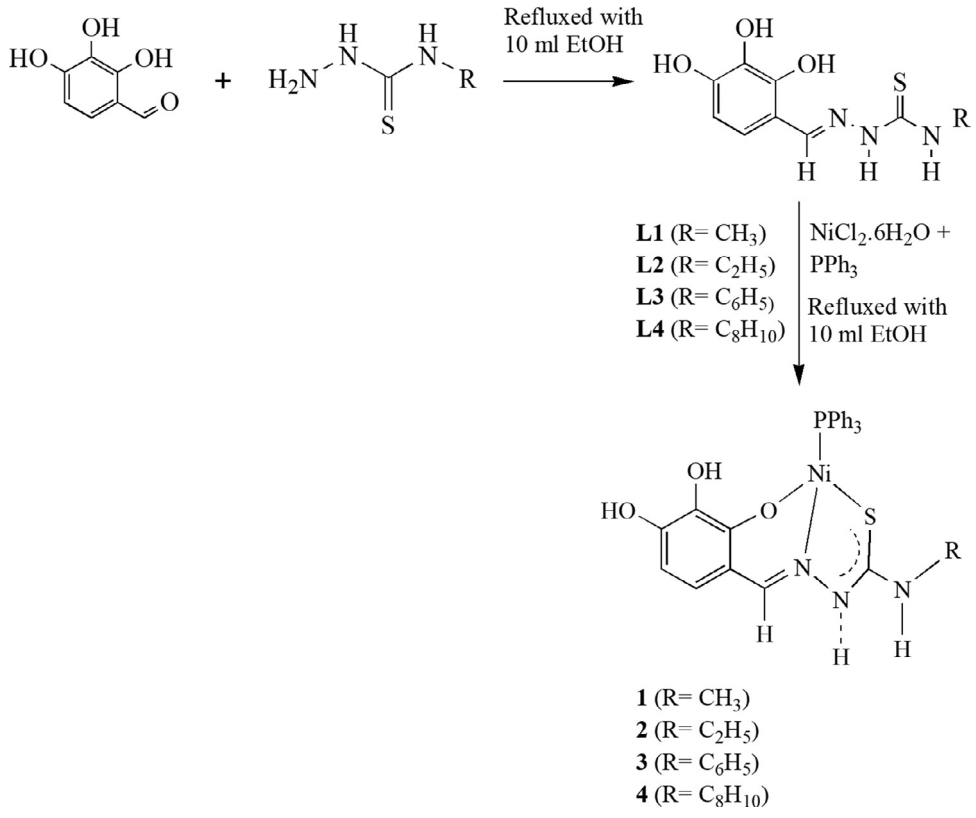

Scheme 1. Schematic representation for the synthesis of ligands (L1-L4) and complexes (1–4).

Table 1
Infrared spectra of ligands (L1-L4) and complexes (1–4).

Compd.	CH=*N*	*C* = *S*/C-S	N(2)H	*v*(cm^{-1}) N(3)H	OH	Ni-S	Ni-N	Ni-O	PPh_3
L1	1637	1346/823	3180	3202	3452	–	–	–	–
L2	1632	1348	3170	3349	3439	–	–	–	–
L3	1612	/7,981,345	3149	3441	3531	–	–	–	–
L4	1634	/8,041,378	3140	3341	3352	–	–	–	–
1	1616	/8,331,380/788	3169	3310	3427	488	533	509	1434 1084 689
2	1610	1320	3161	3454	3218	494	528	503	1435 1091 691
3	1562	/7,791,318	–	3370	3448	489	529	507	1436 1093 690
4	1654	/7,651,315/782	–	3439	3534	493	531	510	1436 1095 693

were observed at a range of 1345–1378 cm^{-1} [30]. Besides, the hydrazinic proton *v*(N(3)H) for all ligands were observed at a range of 3202–3441 cm^{-1} [47,48] . The absence of *v*(S-H) band at 2570 cm^{-1} and the presence of the *v*(N(2)H) band at a range of 3140–3180 cm^{-1} indicates that all ligands are in their thione form [49,50]. The *v*(OH) peaks for these ligands were observed at a range of 3352–3531 cm^{-1} [51,52]. Whereas the peaks belonging to *v*(C–O) were observed at a range of 1251–1283 cm-1 [53].

3.2.2. Infrared spectra of metal complexes (**1–4**)

In most cases, the azomethine imine peaks *v*(CH=*N*) of metal complexes would be found to have shifted to lower wavenumbers as is the case in complexes (**1–3**) [54] . However, the mentioned peak was found to have shifted to higher wavenumber in complex **4**. Hence, addition of metal salt can also cause a shift to higher wavenumbers [55]. This confirms the coordination of all ligands to their metal centre through the azomethine imine nitrogen atom. The hydrazinic proton v(N(3)H) in all complexes were found to have shifted to higher wavenumbers and be at a range of 3310–3454 cm^{-1}, indicating that complexation has occurred through the azomethine imine nitrogen atom. However only complexes **1** and **2** showed the presence of *v*(N(2)H) peak at a range of 3161–3169 cm-1, indicating that ligands **L1** and **L2** are coordinated to the metal centre in their initial thione form [56]. The disappearance of the *v*(N(2)H) bands in complexes **3** and **4** presents convincing affirmation that ligands **L3** and **L4** are coordinated to their metal centres in the deprotonated thiolate form. Besides, the emergence of new *v*(Ni-S), *v*(Ni-N) and *v*(Ni-O) at a range of 488–494 cm^{-1}, 528–533 cm^{-1} and 503–510 cm^{-1}, respectively guarantees once again the coordination of ligands to metal centre through their O,N,S tridentate binding sites [57-60]. The *v*(OH) peak for all complexes were observed at a range of 3218–3448 cm^{-1}, suggesting that only one phenolic OH group was involved in metal complexation. The *v*(C–O) peaks in metal complexes were found to be at similar ranges as their free ligands. The bands due to triphenylphosphine after metal complexation for all complexes were found to be at ranges of 1434–1436 cm^{-1}, 1084–1095 cm^{-1} and 689–693 cm^{-1} [53].

3.3. ^{1}H NMR and ^{13}C NMR spectra

3.3.1. 1H NMR and ^{13}C NMR spectra of ligands (**L1-L4**)

Table 2 shows the proton resonance signals of all ligands and complexes whereas the carbon resonance signals are shown in

Table 2
^{1}H NMR spectra of ligands (**L1-L4**) and complexes (**1–4**).

Compd.	CH=*N*	N(2)H	δ(ppm) N(3)H	OH	Aromatic	Aliphatic
L1	8.19 (s, 1H)	11.19 (s, 1H)	8.41(s, 1H)	9.53 (s, 1H) 8.96 (s, 1H) 8.23 (d, 1H)	6.32–7.12	2.95 (d, CH_3)
L2	8.19 (s, 1H)	11.20 (s, 1H)	8.26 (t, 1H)	9.55 (s, 1H) 8.99 (s, 1H) 8.43 (s, 1H)	6.32–7.11	3.53 (q, CH_2) 1.08 (t, CH_3)
L3	8.31 (s, 1H)	11.56 (s, 1H)	8.46 (s, 1H)	9.89 (s, 1H) 9.58 (s, 1H) 6.34 (d, 1H)	7.13–7.54	-
L4	8.33 (s, 1H)	11.51 (s, 1H)	9.65 (s, 1H)	9.84 (d, 1H) 6.49 (d, 1H) 6.37 (d, 1H)	7.10–7.44	2.59 (q, CH_2) 1.17 (t, CH_3)
1	8.19 (s, 1H)	11.17 (s, 1H)	8.23 (s, 1H)	6.46 (d, 1H) 6.32 (d,1H)	7.04–7.58	2.93 (d, CH_3)
2	8.18 (s, 1H)	11.10 (s, 1H)	8.27 (s, 1H)		7.11–7.42	1.27 (q, CH_2) 1.06 (t, CH_3)
3	8.45 (d, 1H)	-	9.25 (s, 1H)		6.85–7.76	-
4	8.40 (d, 1H)	-	9.14 (s, 1H)		6.82–7.74	2.45 (q, CH_2) 1.08 (t, CH_3)
				6.33 (d, 1H) 6.05 (s, 1H) 9.25 (s, 1H) 6.21 (d, 1H) 9.21 (s, 1H) 6.17 (d, 1H)		

Table 3
^{13}C NMR spectra of ligands (**L1-L4**) and complexes (**1–4**).

Compd.	*C* = *N*	*C* = *S*	δ(ppm) C–O	Aromatic	Aliphatic
L1	141.87	177.51	133.20–148.62	108.43–118.45	31.33 (CH_3)
L2	142.01	176.44	133.20–148.64	108.16–118.54	38.76 (CH_2) 15.23 (CH_3)
L3	147.19	175.54	148.90–153.76	108.19–142.80	–
L4	147.16	175.59	148.85–153.76	108.18–140.99	28.18 (CH_2) 16.17 (CH_3)
1	141.65	177.29	134.08–148.59	108.26–133.15	31.42 (CH_3)
2	141.45	176.35	134.04–148.60	108.23–133.42	38.78 (CH_2) 15.22 (CH_3)
3	164.87 164.70	-	146.48–153.06	107.86–141.92	-
4	164.84 164.67	-	146.39–153.06	107.81–139.75	28.04 (CH_2) 16.38 (CH_3)

Table 3. The singlet proton resonance signal belonging to the azomethine imine group (CH=*N*) was seen to be at a range of 8.19–8.33 ppm for all ligands [61]. The fact that all ligands are in their thioamide form is proved by the absence of resonance signal at around 4 ppm which belongs to the (S-H) group [50]. The presence of all ligands in their thioamide form is further confirmed by the appearance of singlet proton resonance signal at a range of 11.12–11.56 ppm which belongs to the thiohydrazinic proton (N(2)H) [62-64]. The hydrazinic (N(3)H) proton resonance signal for all ligands were found to be at a range of 8.26–9.65 ppm and the shift in resonance signal is highly dependant on the substituent group attached to it [65,66]. The resonance signal for aromatic ring which appeared as multiplets were observed at a range of 6.32–9.89 ppm for all ligands [67]. Also, the phenolic OH resonance signal was observed at a range of 6.34- 9.89 ppm [68,69]. Whilst, the aliphatic proton resonance signals due to -CH_2 and -CH_3 groups were seen to be at a range of 2.95–3.53 ppm and 1.08–2.95 ppm for all ligands [70].

Carbon resonance signals showed by azomethine imine nitrogen (*C* = *N*) for all ligands were observed at a range of 141.87–147.19 ppm. The resonance signal for thioamide (*C* = *S*) were found to be at a range of 175.54–177.51 for all ligands, stipulating that the ligands are in their thione form [71]. Besides, the resonance signal for phenolic OH were detected at a range of 133.20–153.76 ppm. Whilst, the resonance signals caused by aromatic carbons were observed at 108.14–142.80 ppm [72]. Whereas, resonance signals due to aliphatic carbons caused by -CH_2 group and -CH_3 group were spotted at 28.18–38.76 ppm and 15.23–31.38 ppm, respectively [73-75]. The total number of carbon resonance signals from the spectra were in tandem with the proposed structures of all ligands.

3.3.2. ^{1}H NMR and ^{13}C NMR spectra of metal complexes (*1–4*)

The azomethine imine nitrogen (CH=*N*) resonance signal was found to have shifted slightly downfield and resonate at a range of 8.18–8.45 ppm, proving that the ligands are coordinated to the metal centre via their azomethine imine nitrogen atom. The azomethine resonance signal for complexes **3** and **4** were observed as doublets due to coupling with phosphorus atom of triphenylphosphine [76]. Complexes **1** and **2** show resonance signals due to thiohydrazinic proton (N(2)H) at 11.17 ppm and 11.10 ppm, respectively. Hence, ligands **L1** and **L2** were found to have coordinated to the metal centre in their thioamide form. However, resonance signal at this range was absent in complexes **3** and **4**, indicating that ligands **L3** and **L4** were coordinated to the metal centre in their thiolate form. This is further confirmed by the emergence of a new resonance signal belonging to the (S-H) group at 4.70 ppm and 4.68 ppm for complexes **3** and **4**, respectively. The hydrazinic proton resonance signal (N(3)H) was seen to have

shifted downfield in complexes **2** and **3** as a result of decrease in electron density due to the electron withdrawal by metal centre, sulphur, and deprotonated phenolic OH [77]. However, complexes **1** and **4** were seen to not follow this trend as occasional change in trend is common. The resonance signal due to phenolic OH in all complexes were observed at a range of 6.05–9.25 ppm, similar as their ligands, suggesting that only one phenolic OH group was involved in metal complexation. Resonance signals of aromatic protons in all complexes were found to resonate at similar resonances as their ligands because aromatic protons were not affected by metal complexation. There isn't much variation in the resonance signals produced by aliphatic protons in all complexes from their respective ligands because aliphatic protons are not involved in metal complexation as well.

Since the azomethine imine nitrogen ($C = N$) is involved in metal complexation, their resonance signals were observed at 141.65 ppm and 141.45 ppm for complexes **1** and **2**, respectively. Their thioamide carbon resonance signals ($C = S$) were spotted at 177.29 ppm and 176.35 ppm, indicating that ligands **L1** and **L2** were coordinated to the metal centre in their initial thione form. Furthermore, a slight upfield shift in the thioamide resonance signal observed in complexes **1** and **2** is due to lowering of C-S bond order as a result of metal complexation [78]. However, complexes **3** and **4** produced resonance signals at a range of 164.67–164.87 ppm which belongs to the azomethine imine nitrogen ($C = N$). This downfield shift of the mentioned group reaffirms the coordination of ligands **L3** and **L4** to the metal centre via their azomethine imine nitrogen atom. Besides, the resonance signal due to thioamide carbon was absent in these complexes, confirming that ligands **L3** and **L4** were coordinated to the metal centre in the thiolate form. The resonance signal caused by phenolic OH was spotted at a range of 146.39–150.25 ppm, denoting that only one of the phenolic OH was involved in metal complexation. Significant changes were not observed in the resonance signals produced by aromatic and aliphatic carbon atoms. Once again, the number of carbon atoms from the spectra were in tandem with the proposed structures for all complexes.

3.4. Crystal structures

The crystal data and refinement parameters of complexes (**1–3**) are shown in Table 4. However, the crystal data of complex **4** could not be produced although it was successfully synthesised. Whereas, Table 5 shows the selected bond lengths and bond angles of complex **1**. Selected bond lengths and bond angles of complexes **2** and **3** are shown in Supplementary Information (Table A. 1- Table A. 2). Meanwhile, the crystal structures of complexes (**1–3**) are shown in Fig. 2 whereas the unit cell packing of complex **1** is shown in Fig. 3. The unit cell packing of complexes **2** and **3** are shown in Supplementary Information (Fig. A. 1- Fig. A. 2).

3.4.1. Crystal structures of complexes (*1–3*)

It is revealed by single crystal X-ray analysis that complexes **1** and **2** crystallised in triclinic crystal system with P1 space group. Whilst, complex **3** was found to have crystallised into a monoclinic lattice with $P2_1$ space group. All three complexes were four coordinated and displays a square planar geometry. All ligands were found to have coordinated to the metal centre via their O,N,S tridentate binding site. The S1-C8 bond lengths for complexes **1, 2** and **3** were seen at 1.721 (3) Å, 1.714 (3) Å and 1.728 (12) Å, respectively. The bond lengths are similar as those observed in other thiosemicarbazone metal complexes. It is noteworthy that the S1-C8 bond lengths for complexes **1** and **2** were shorter than complex **3**, indicating that the mentioned bond is a double bond in complexes **1** and **2** but a single bond in complex **3** [79]. The fact that

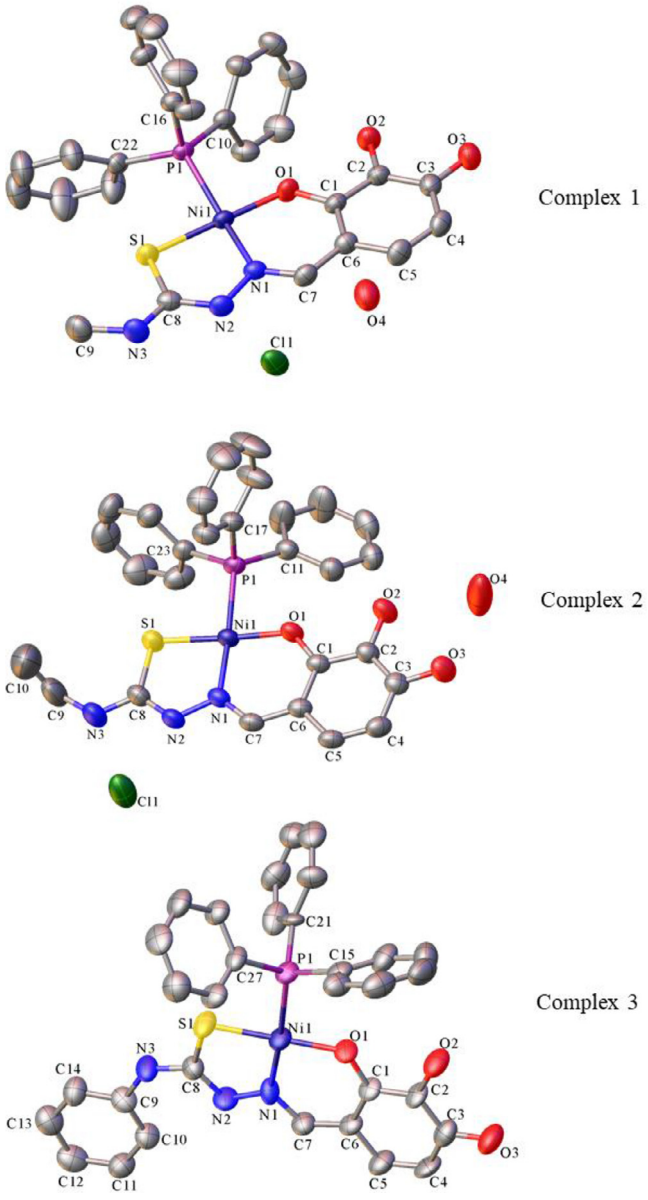

Fig. 2. Ellipsoid plots of complexes (**1–3**). Hydrogen atoms are omitted and some of the atoms are not labelled for clarity.

coordination gives rise to an increase of the single bond character for C-S bond is true in the case of complex **3** [80]. Besides, the effect of thione to thiol tautomerization is clearly observed in complex **3.** In addition, the N2-C8 bond lengths were seen at 1.324 (4) Å, 1.328 (4) Å and 1.299 (14) Å for complexes **1, 2** and **3**, respectively. It is interesting to note that the N2-C8 bond lengths for complexes **1** and **2** were longer than complex **3**, suggesting that the mentioned bond is a single bond in complexes **1** and **2** but a double bond in complex **3** [81]. Similar bond lengths were observed in thiosemicarbazones reported by previous researches, stipulating that ligands **L1** and **L2** were coordinated to the metal in the original thione form but ligand **L3** was coordinated to the metal in its thiolate form. The bite angle for O1-Ni1-N1, N1-Ni-S1, S1-Ni-P1 and O1-Ni-P1 which slightly deviate from the ideal 90 ° reflect that the complexes adopt a distorted square planar geometry. Deviations due to restricted bite angle caused by ligands is common [58,82]. Besides, the O1-Ni-S1 and N1-Ni-P1 bonds were found to intersect at an approximate angle of 180 ° signifying

Table 4
Crystallographic data summary for complexes (**1–3**).

Compounds	1	2	3
Empirical formula	$C_{27}H_{27}ClN_3NiO_4PS$	$C_{28}H_{28}ClN_3NiO_4PS$	$C_{32}H_{27}N_3NiO_3PS$
Formula weight	614.70	627.69	623.30
Crystal system	Triclinic	Triclinic	Monoclinic
Space group	*P*1	*P*1	$P2_1$
Unit cell dimensions	9.5562 (4)	7.9432 (5)	9.6016 (3)
a (Å)	12.7600 (5)	14.000 (1)	10.6957 (3)
b (Å)	13.0135 (7)	14.2845 (9)	13.5895 (6)
c (Å)	97.172 (4)	91.597 (5)	93.499 (3)
β (°)	1387.92 (12)	1448.59 (18)	1392.98 (8)
V (Å^3)	2	2	2
Z	636	615	646
F(000)	1.471	1.360	1.486
D_{calc} (mg m^{-3})	3.46	2.86	2.58
Absorption coefficient, μ (mm^{-1})	293	293	293
T (K)	0.10 × 0.10 × 0.05	0.10 × 0.10 × 0.05	0.10 × 0.10 × 0.05
Crystal size (mm)	8175	8468	2486
Reflections collected	5313 (0.033)	5533 (0.029)	1618 (0.031)
Independent reflections (R_{int})	5313/0/349	5533/0/358	1618/1/372
Data/restraints/parameters	0.054	0.053	0.044
$R[F^2 > 2\sigma(F^2)]$	0.151	0.159	0.125
$wR(F^2)$	1.03	1.03	1.10
S	0.97 and −1.08	0.68 and −0.66	0.43 and −0.44
Largest differencepeak and hole (e Å^{-3})			

Table 5
Selected bond lengths (Å) and bond angles (°) for complex **1.**

Bond lengths (Å)		Bond angles (°)	
Ni1—P1	2.206 (7)	S1—Ni1—P1	90.27 (3)
Ni1—S1	2.148 (7)	O1—Ni1—P1	88.06 (6)
Ni1—O1	1.849 (19)	O1—Ni1—S1	175.68 (8)
Ni1—N1	1.881 (2)	O1—Ni1—N1	94.09 (9)
S1—C8	1.721 (3)	N1—Ni1—P1	168.04 (7)
N1—N2	1.394 (3)	N1—Ni1—S1	88.35 (7)
N1—C7	1.310 (3)	C16—P1—Ni1	107.92 (9)
N2—C8	1.324 (4)	C22—P1—C10	107.68 (12)
N3—C8	1.323 (3)	C10—P1—Ni1	112.51 (8)
N3—C9	1.446 (4)	C22—P1—Ni1	116.75 (8)

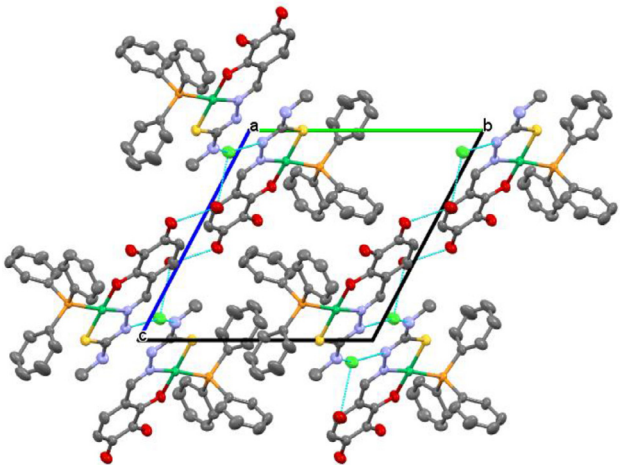

Fig. 3. Unit cell packing diagram of complex **1**. Water molecules and chloride ions bridge the adjacent ligands. Intermolecular O–H—Cl, O–H—O and N–H—Cl hydrogen bonding observed.

that all complexes are in a distorted square planar geometry. Each molecule of complex **1** is involved in intermolecular O–H—O and N–H—Cl hydrogen bonding interactions. The water molecule and chlorine ion served as a bridge to the adjacent ligand through a network of hydrogen bonding interactions leading to the formation of a parallel linear chain. The packing of the molecules is stabilised by a combination of hydrogen bonding and Van der Waals interaction leading to a 2-dimension network along the c-axis (Fig. 3). Complex **2** is linked by intermolecular O–H—Cl, O–H—O and N–H—Cl hydrogen leading to the formation of parallel chain along the a-axis (**Figure A1 SI**). No hydrogen bonding was observed for complex **3**, the packing of the molecules was stabilised by the Van der Waals interaction between the phenyl ring of the triphenylphosphine moiety and the phenyl substituent on the nitrogen atom, leading to the formation of a zig-zag chain along the b-axis (**Figure A2 SI**).

*3.5. Cytotoxic activity of ligands (**L1**–**L4**) and metal complexes (**1**–**4**)*

The cytotoxicity of the ligands and metal complexes was tested against three human cancer cell lines, namely PC-3, HCT 116, and MCF7, and the results are reported in Table 6. Ligand **L1** was inactive against PC-3 but showed a moderate cytotoxic activity against HCT 116 and MCF7 with IC_{50} 10.34 ± 0.23 and 11.79 ± 0.86 μM, respectively. Ligand **L2** exhibited a potent growth inhibitory effect against HCT 116 with an IC_{50} 5.75 ± 0.49 μM, which is comparable with cisplatin (IC_{50} 5.92 ± 0.79 μM), and it also showed a substantial cytotoxicity against MCF7 with an IC_{50} 8.68 ± 0.11 μM. Both ligands **L3** and **L4** displayed a stronger cytotoxicity than cisplatin with IC_{50} 9.82 ± 0.69 and 15.66 ± 2.44 μM, respectively when tested against PC-3, and they exhibited moderate growth inhibitory effect when tested against HCT 116 (**L3**, IC_{50} 9.82 ± 1.85 μM; **L4**, IC_{50} 9.75 ± 0.54 μM). Overall, **L2** exhibited a wider spectrum of cytotoxicity than the other ligands with reference to the result of HCT 116 and MCF7. This is consistent with the previous study that the addition of long aliphatic and lipophilic side chain could en-

Table 6
In vitro cytotoxic activity (IC_{50} values) of ligands (**L1-L4**) and complexes (**1–4**) against three human cancer cell lines.

Compound	PC-3	IC_{50} in μM HCT 116	MCF7
L1	>100	10.34 ± 0.23	11.79 ± 0.86
L2	82.47 ± 4.14	5.75 ± 0.49	8.68 ± 0.11
L3	9.82 ± 0.69	9.82 ± 1.85	29.70 ± 0.16
L4	15.66 ± 2.44	9.75 ± 0.54	23.80 ± 1.54
1	>100	4.26 ± 0.29	13.03 ± 0.69
2	>100	12.68 ± 0.72	24.72 ± 1.59
3	>100	7.07 ± 0.61	>100
4	>100	>100	>100
Cisplatin*	19.45 ± 0.73	5.92 ± 0.79	4.38 ± 0.50

* Positive control, cisplatin was used as a reference standard. Values were expressed as mean ± standard deviation ($n = 3$).

Table 7
IC_{50} (μM) values for *P. falciparum 3D7*.

Compound	IC_{50} (μM)[a]
L1	>25[b]
L2	>25[b]
L3	>25[b]
L4	>25[b]
1	>25[b]
2	9.88 ± 0.23
3	1.06 ± 0.01
4	>25[b]
Chloroquine*	(3.25 ± 0.23) x 10^{-3}

* Positive control.
[a] Mean (±SD) from two different experiments which were performed in duplicates each.
[b] $R^2 < 0.8$.

hance the cytotoxicity of the compound (**L2**), while the introduction of aromatic ring into the compound (**L3** and **L4**) has no significant improvement to the cytotoxicity [83].

Generally, our results showed that the complexation did not improve the cytotoxicity of the parent ligands, except for complexes **1** and **3**. Notably, the complexation of **L1** has significantly enhanced the cytotoxicity of **1** against HCT 116 to an extent that becoming more potent than cisplatin with an IC_{50} 4.26 ± 0.29 μM. Interestingly, the complexation of **L3** has slightly increased the cytotoxicity and cell line-specificity of the complex **3** towards HCT 116 (IC_{50} 7.07 ± 0.61 μM). Complex **3** is more hydrophobic than **2**, therefore, it exhibited a stronger cytotoxic activity than the latter (IC_{50} 12.68 ± 0.72 μM) when tested against HCT 116, indicating once again that cytotoxicity is directly proportional to hydrophobicity [84]. In general, cytotoxicity increases as the lipophilicity of the alkyl residue at the N3 nitrogen atom increases [85].

3.6. Antiplasmodium activity of ligands (*L1–L4*) and metal complexes (*1–4*)

The Table 7 reports the IC_{50} of the compounds and the goodness of fit of each result, whether it is more or lesser than 0.8. All ligands were inactive against *P. falciparum*, while the complexation of **L2** and **L3** into complexes **2** and **3** has gained pronounced antimalarial activity with IC_{50} 9.88 ± 0.23 μM and 1.06 ± 0.01 μM, respectively. Similar to the MTT cytotoxicity study, **3** has a higher antimalarial activity than **2**, which again probably due to the higher hydrophobicity of **3** than the latter [86]. In contrast with complex **3**, complex **4** is inactive although **4** is also hydrophobic, suggesting that the antimalarial activity can only be improved when the hydrophobicity is attributed by phenyl group (in **3**) but not the longer and larger ethyl phenyl group (in **4**), as the latter tend to lower the activity [87].

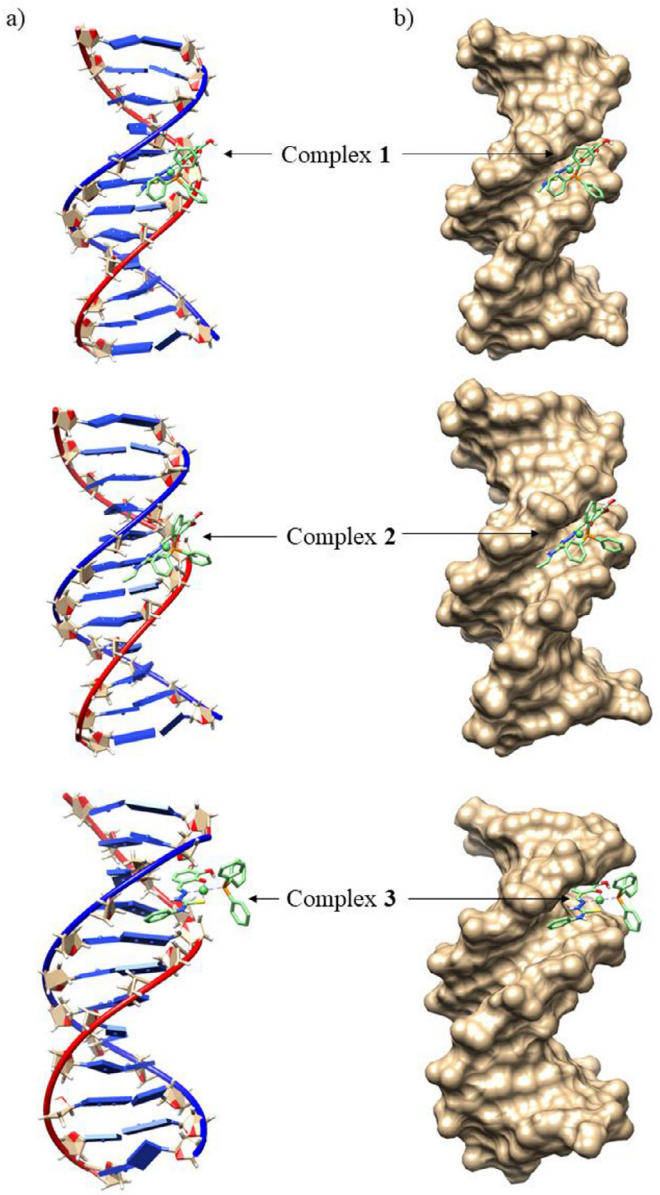

Fig. 4. Molecular docking simulatSSions showing the interactions between complexes and 1BNA where a) ribbon model and b) molecular surface of 1BNA.

3.7. Molecular docking studies

The DNA binding affinity of the bioactive complexes **1–3** was assessed using molecular docking simulations with an attempt to investigate the cytotoxicity and antiplasmodial mechanisms of the complexes. Fig. 4 and Fig. 5 show the interactions of these complexes with DNA duplex 1BNA and 1XRW, respectively. The complexes were found to fit into the DNA minor groove instead of intercalating between the DNA, probably due to their increased molecular size as a result of complexation that unfavours intercalation. A closer examination into the DNA-complex interactions revealed hydrophobic interactions of the benzaldehyde, triphenylphosphine, and phenyl moieties with DNA base pairs. The DNA binding strength of the complexes was inferred from the binding energy, whereby the estimated binding energy for complexes **1, 2, 3** are −7.3, −8.5, and −8.4 $kcalmol^{-1}$, respectively. The binding energy of these complexes are comparable to those previously reported active DNA surface binders [88,89], suggesting that the

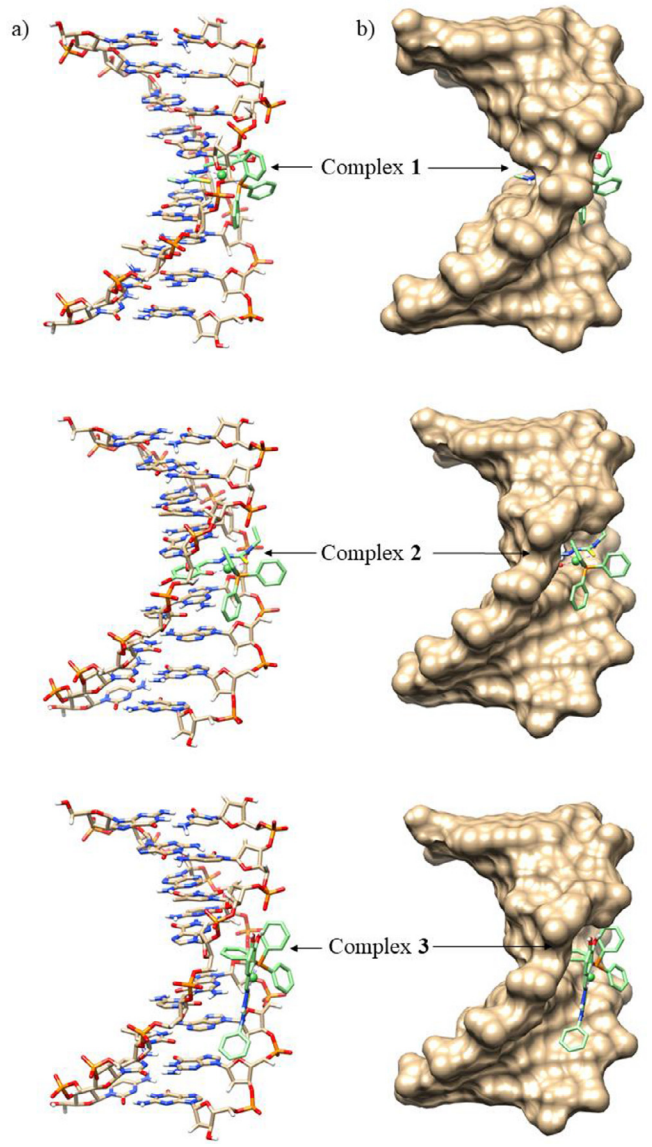

Fig. 5. Molecular docking simulation showing the interaction between complexes and 1XRW where a) ribbon model and b) molecular surface of 1XRW.

complexes **1**–**3** have a strong DNA binding affinity. Evidently, the DNA binding strength of these complexes increases in the order of **1** < **3** < **2**, with complexes **2** and **3** being strong DNA binders, which reflected its potent cytotoxicity in HCT 116 (Table 6) and antiplasmodial activity (Table 7).

4. Conclusion

The cytotoxicity and antimalarial activity of a compound are featured by the role played by the substituent at the N(3) position. In this case, compounds with a molecular weight of less than 627 g/mol were found to be cytotoxic and show antimalarial properties. However, this is not always true as anomalies in trend may occur. Complexes **1, 3** and ligand **L2** could be developed as polyhydroxybenzaldehyde based anticancer agents. Notably, our complexation process has significantly enhanced the biological activities of the ligands, as observed in complexes **2** and **3**. Complexes **2** and **3** could be developed as candidates for studying antimalarial activity, and the latter was found to exhibit both cytotoxicity and antimalarial activity. Molecular docking reveals the binding of complexes **1**–**3** at the minor groove where their benzaldehyde, triphenylphosphine, aliphatic chain and phenyl moieties interact with DNA base pairs. In future, much focus and importance should be given to compounds similar to complexes **2** and **3** in the development of a single drug with cytotoxic and antimalarial properties.

Declaration of Competing Interest

The authors declare that they have no known competing financial interests or personal relationships that could have appeared to influence the work reported in this paper.

CRediT authorship contribution statement

Savina Savir: Writing - original draft, Validation, Investigation, Visualization, Data curation, Methodology, Conceptualization. **Jonathan Wee Kent Liew:** Validation, Investigation. **Indra Vythilingam:** Writing - review & editing, Supervision. **Yvonne Ai Lian Lim:** Writing - review & editing, Supervision. **Chun Hoe Tan:** Validation, Investigation. **Kae Shin Sim:** Writing - review & editing, Supervision. **Vannajan Sanghiran Lee:** Writing – review & editing. **Mohd. Jamil Maah:** Writing - review & editing, Supervision. **Kong Wai Tan:** Writing - review & editing, Supervision.

Acknowledgements

This work is supported by the University of Malaya Research Grant (grant number RP033A-17AFR), MOHE (FRGS-FP006–2015A) and MyBrain Scholarship. Special thanks to Prof. Ng Seik Weng for his help and support in this project.

Supplementary materials

Supplementary material associated with this article can be found, in the online version, at doi:10.1016/j.molstruc.2021.130815.

References

[1] F. Bray, et al., Global cancer statistics 2018: GLOBOCAN estimates of incidence and mortality worldwide for 36 cancers in 185 countries, CA Cancer J. Clin 68 (6) (2018) 394–424.
[2] B. Rosenberg, L. Van Camp, T. Krigas, Inhibition of cell division in Escherichia coli by electrolysis products from a platinum electrode, Nature 205 (4972) (1965) 698–699.
[3] D. Lebwohl, R. Canetta, Clinical development of platinum complexes in cancer therapy: an historical perspective and an update, Eur. J. Cancer 34 (10) (1998) 1522–1534.
[4] S. Ishida, et al., Uptake of the anticancer drug cisplatin mediated by the copper transporter Ctr1 in yeast and mammals, Proceed. National Acad. Sci. 99 (22) (2002) 14298–14302.
[5] S. Dasari, P.B. Tchounwou, Cisplatin in cancer therapy: molecular mechanisms of action, Eur. J. Pharmacol. 740 (2014) 364–378.
[6] X. Wang, Z. Guo, Targeting and delivery of platinum-based anticancer drugs, Chem. Soc. Rev. 42 (1) (2013) 202–224.
[7] Liu, et al., Antimalarial drug pyrimethamine plays a dual role in antitumor proliferation and metastasis through targeting DHFR and TP, Mol. Cancer Ther. 18 (3) (2019) 541–555.
[8] K.A. Koram, M.E. Molyneux, When is “malaria” malaria? The different burdens of malaria infection, malaria disease, and malaria-like illnesses, Am. J. Trop. Med. Hyg 77 (6) (2007) 1–5.
[9] O. World Health, World Malaria Report, World Health Organization, Geneva, 2019 2019.
[10] A. Boudhar, et al., Overcoming chloroquine resistance in malaria: design, synthesis and structure–activity relationships of novel chemoreversal agents, Eur. J. Med. Chem. 119 (2016) 231–249.
[11] J.E. Hyde, Drug-resistant malaria, Trends Parasitol 21 (11) (2005) 494–498.
[12] A.C. Aguiar, et al., Chloroquine analogs as antimalarial candidates with potent in vitro and in vivo activity, Int. J. Parasitol.: Drugs and Drug Resistance 8 (3) (2018) 459–464.
[13] C. Biot, et al., Structure–activity relationships of 4-N-substituted ferroquine analogues: time to re-evaluate the mechanism of action of ferroquine, J. Organomet. Chem. 694 (6) (2009) 845–854.

[14] J. Held, et al., Ferroquine and artesunate in African adults and children with Plasmodium falciparum malaria: a phase 2, multicentre, randomised, double-blind, dose-ranging, non-inferiority study, The Lancet Infectious Diseases 15 (12) (2015) 1409–1419.
[15] G. Mombo-Ngoma, et al., Phase I randomized dose-ascending placebo-controlled trials of ferroquine-a candidate anti-malarial drug-in adults with asymptomatic Plasmodium falciparum infection, Malar. J. 10 (1) (2011) 53.
[16] B. Şen, et al., Crystal structures, spectroscopic properties of new cobalt (II), nickel (II), zinc (II) and palladium (II) complexes derived from 2-acetyl-5-chloro thiophene thiosemicarbazone: anticancer evaluation, Mater. Sci. Eng.: C 98 (2019) 550–559.
[17] J.S. Casas, et al., Diorganotin (IV) complexes of pyridoxal thiosemicarbazone: synthesis, spectroscopic properties and biological activity, J. Inorg. Biochem. 69 (4) (1998) 283–292.
[18] B.M. Paterson, P.S. Donnelly, Copper complexes of bis (thiosemicarbazones): from chemotherapeutics to diagnostic and therapeutic radiopharmaceuticals, Chem. Soc. Rev. 40 (5) (2011) 3005–3018.
[19] R. Matsa, et al., Thiosemicarbazone derivatives: design, synthesis and in vitro antimalarial activity studies, Eur. J. Pharmaceut. Sci. 137 (2019) 104986.
[20] F. Bisceglie, et al., Copper (II) thiosemicarbazonate molecular modifications modulate apoptotic and oxidative effects on U937 cell line, J. Inorg. Biochem. 116 (2012) 195–203.
[21] Y. Kaya, A. Erçağ, A. Koca, New square-planar nickel (II)-triphenylphosphine complexes containing ONS donor ligands: synthesis, characterization, electrochemical and antioxidant properties, J. Mol. Struct. 1206 (2020) 127653.
[22] M. Shabbir, et al., Nickel (II) and palladium (II) triphenylphosphine complexes incorporating tridentate Schiff base ligands: synthesis, characterization and biocidal activities, J. Mol. Struct. 1149 (2017) 720–726.
[23] M. Chrysouli, et al., Chloro (triphenylphosphine) gold (I) a forefront reagent in gold chemistry as apoptotic agent for cancer cells, J. Inorg. Biochem. 179 (2018) 107–120.
[24] K. Aswin, et al., Triphenylphosphine: an efficient catalyst for the synthesis of 4, 6-diphenyl-3, 4-dihydropyrimidine-2 (1H)-thione under thermal conditions, J. King Saud University-Sci. 26 (2) (2014) 141–148.
[25] M. Navarro, et al., The mechanism of antimalarial action of [Au (CQ)(PPh3)] PF6: structural effects and increased drug lipophilicity enhance heme aggregation inhibition at lipid/water interfaces, J. Inorg. Biochem. 105 (2) (2011) 276–282.
[26] S. Deshpande, et al., Topological descriptors in modelling antimalarial activity: n 1-(7-chloro-4-quinolyl)-1, 4-bis (3-aminopropyl) piperazine as prototype, J. Enzyme Inhib. Med. Chem 24 (1) (2009) 94–104.
[27] J.-.L. Qin, et al., Oxoaporphine metal complexes (Co II, Ni II, Zn II) with high antitumor activity by inducing mitochondria-mediated apoptosis and S-phase arrest in HepG2, Sci. Rep. 7 (2017) 46056.
[28] P. Chellan, et al., Cyclopalladated complexes containing tridentate thiosemicarbazone ligands of biological significance: synthesis, structure and antimalarial activity, J. Organomet. Chem. 695 (19) (2010) 2225–2232.
[29] D. Bahl, et al., Structure–activity relationships of mononuclear metal–thiosemicarbazone complexes endowed with potent antiplasmodial and antiamoebic activities, Biorg. Med. Chem. 18 (18) (2010) 6857–6864.
[30] H.B. Shawish, et al., Nickel (II) complexes of polyhydroxybenzaldehyde N4-thiosemicarbazones: synthesis, structural characterization and antimicrobial activities, Transition Met. Chem. 39 (1) (2014) 81–94.
[31] H.B. Shawish, M.J. Maah, S.W. Ng, 1-(2, 3, 4-Trihydroxybenzylidene)-4-ethylthiosemicarbazide, Acta Crystallogr. Sect. Sect. E: Struct. Rep. Online 66 (5) (2010) o1151 o1151.
[32] M.A.G. Gomes, et al., Evaluating anti-Toxoplasmagondii activity of new serie of phenylsemicarbazone and phenylthiosemicarbazones in vitro, Med. Chem. Res. 22 (8) (2013) 3574–3580.
[33] S. Savir, et al., Synthesis, cytotoxicity and antimalarial activities of thiosemicarbazones and their nickel (II) complexes, J. Mol. Struct. (2020) 128090.
[34] O.V. Dolomanov, et al., OLEX2: a complete structure solution, refinement and analysis program, J. Appl. Crystallogr. 42 (2) (2009) 339–341.
[35] G. Sheldrick, Crystal structure refinement with SHELXL, Acta Crystallographica Section C 71 (1) (2015) 3–8.
[36] C.F. Macrae, et al., Mercury CSD 2.0 - new features for the visualization and investigation of crystal structures, J. Appl. Crystallogr. 41 (2) (2008) 466–470.
[37] S. Westrip, publCIF: software for editing, validating and formatting crystallographic information files, J. Appl. Crystallogr. 43 (4) (2010) 920–925.
[38] F.A. Fatih, et al., Susceptibility of human Plasmodium knowlesi infections to anti-malarials, Malar. J. 12 (1) (2013) 425.
[39] V. Kosaisavee, et al., Plasmodium vivax: isotopic, PicoGreen, and microscopic assays for measuring chloroquine sensitivity in fresh and cryopreserved isolates, Exp. Parasitol. 114 (1) (2006) 34–39.
[40] B. Russell, et al., Determinants of in vitro drug susceptibility testing of Plasmodium vivax, Antimicrob. Agents Chemother. 52 (3) (2008) 1040–1045.
[41] O. Trott, A.J. Olson, AutoDock Vina: improving the speed and accuracy of docking with a new scoring function, efficient optimization, and multithreading, J. Comput. Chem. 31 (2) (2010) 455–461.
[42] H.R. Drew, et al., Structure of a B-DNA dodecamer: conformation and dynamics, Proceedings of the National Acad. Sci. 78 (4) (1981) 2179–2183.
[43] H. Baruah, M.W. Wright, U. Bierbach, Solution structural study of a DNA duplex containing the Guanine-N7 adduct formed by a cytotoxic platinum– acridine hybrid agent, Biochemistry 44 (16) (2005) 6059–6070.
[44] E.F. Pettersen, et al., UCSF Chimera—A visualization system for exploratory research and analysis, J. Comput. Chem. 25 (13) (2004) 1605–1612.
[45] H.B. Shawish, M.J. Maah, S.N.A. Halim, Synthesis and characterization of mixed nickel thiosemicarbazone complexes, Malays. J. Fundamen. Appl. Sci. 8 (3) (2012).
[46] G. Arutyunyan, et al., Synthesis and conversions of polyhedral compounds. 32. Synthesis and antibacterial activity of azaadamantane-containing azomethine dihydrochlorides, Pharm. Chem. J. 52 (5) (2018) 419–423.
[47] M. Munakata, et al., 1-D cyano-bridged heterometallic complexes consisting of 1, 4, 8, 11-tetraazacyclotetradecanesilver (II) and tetracyanopalladium (II) or tetracyanoplatinum (II), Inorg. Chim. Acta 317 (1–2) (2001) 268–275.
[48] M. Marchewka, et al., Crystal structure, vibrational spectra and nonlinear optical properties of L-histidinium-L-tartrate hemihydrate, J. Mol. Struct. 656 (1–3) (2003) 265–273.
[49] E.M. Jouad, et al., Synthesis, structural and spectral studies of 5-methyl 2-furaldehyde thiosemicarbazone and its Co, Ni, Cu and Cd complexes, Polyhedron 20 (1–2) (2001) 67–74.
[50] K.W. Tan, et al., Towards a selective cytotoxic agent for prostate cancer: interaction of zinc complexes of polyhydroxybenzaldehyde thiosemicarbazones with topoisomerase I, Polyhedron 38 (1) (2012) 275–284.
[51] J. Liu, et al., The mineral tooeleite Fe6 (AsO3) 4SO4 (OH) 4· 4H2O–An infrared and Raman spectroscopic study-environmental implications for arsenic remediation, Spectrochimica Acta A 103 (2013) 272–275.
[52] B. Weckler, H. Lutz, Near-infrared spectra of M (OH) Cl (M= Ca, Cd, Sr), Zn (OH) F, γ-Cd (OH) 2, Sr (OH) 2, and brucite-type hydroxides M (OH) 2 (M= Mg, Ca, Mn, Fe, Co, Ni, Cd), Spectrochimica Acta A. 52 (11) (1996) 1507–1513.
[53] H.B. Shawish, et al., Nickel (II) complex of polyhydroxybenzaldehyde N4-thiosemicarbazone exhibits anti-inflammatory activity by inhibiting NF-κB transactivation, PLoS ONE 9 (6) (2014) e100933.
[54] S.N. Kotkar, H.D. Juneja, Synthesis, Characterization, and Antimicrobial Studies of N, O Donor Schiff Base Polymeric Complexes, J Chem (2013) 5 **2013**.
[55] K. Andiappan, et al., In vitro cytotoxicity activity of novel Schiff base ligand–lanthanide complexes, Sci. Rep. 8 (1) (2018) 3054.
[56] T.S. Lobana, et al., Bonding and structure trends of thiosemicarbazone derivatives of metals—An overview, Coord. Chem. Rev. 253 (7–8) (2009) 977–1055.
[57] L. Latheef, E. Manoj, M.P. Kurup, Synthesis and spectral characterization of zinc (II) complexes of N (4)-substituted thiosemicarbazone derived from salicylaldehyde: structural study of a novel–OH free Zn (II) complex, Polyhedron 26 (15) (2007) 4107–4113.
[58] E. Seena, M.R.P. Kurup, Spectral and structural studies of mono-and binuclear copper (II) complexes of salicylaldehyde N (4)-substituted thiosemicarbazones, Polyhedron 26 (4) (2007) 829–836.
[59] E. Seena, M.P. Kurup, Synthesis, spectral and structural studies of zinc (II) complexes of salicylaldehyde N (4)-phenylthiosemicarbazone, Spectrochimica Acta A 69 (3) (2008) 726–732.
[60] T. Reena, M.P. Kurup, Copper (II) complexes derived from di-2-pyridyl ketone-N4-phenyl-3-semicarbazone: synthesis and spectral studies, Spectrochimica Acta A 76 (3–4) (2010) 322–327.
[61] M.E. Amato, et al., Synthesis and conformational aspects of 20-and 40-membered macrocyclic mono and dinuclear uranyl complexes incorporating salen and (R)-BINOL units, Tetrahedron 63 (39) (2007) 9751–9757.
[62] Z. Afrasiabi, et al., Appended 1, 2-naphthoquinones as anticancer agents 1: synthesis, structural, spectral and antitumor activities of ortho-naphthaquinone thiosemicarbazone and its transition metal complexes, Inorg. Chim. Acta 357 (1) (2004) 271–278.
[63] J.D. Chellaian, J. Johnson, Spectral characterization, electrochemical and anticancer studies on some metal (II) complexes containing tridentate quinoxaline Schiff base, Spectrochimica Acta A 127 (2014) 396–404.
[64] B.B. Raj, M.P. Kurup, N-2-Hydroxy-4-methoxyacetophenone-N′-4-nitrobenzoyl hydrazine: synthesis and structural characterization, Spectrochimica Acta A 66 (4–5) (2007) 898–903.
[65] L.J. Ackerman, et al., Structural and spectral studies of copper (II) and nickel (II) complexes of pyruvaldehyde mixed bis {N (4)-substituted thiosemicarbazones}, Polyhedron 18 (21) (1999) 2759–2767.
[66] H. Bayrak, et al., Synthesis of some new 1, 2, 4-triazoles, their Mannich and Schiff bases and evaluation of their antimicrobial activities, Eur. J. Med. Chem. 44 (3) (2009) 1057–1066.
[67] A. Çukurovali, et al., Cobalt (II), copper (II), nickel (II) and zinc (II) complexes of two novel Schiff base ligands and their antimicrobial activity, Transition Met. Chem. 27 (2) (2002) 171–176.
[68] M. Tunçel, S. Serin, Synthesis and Characterization of Copper (II), Nickel (II) and Cobalt (II) Complexes with Azo-Linked Schiff Base Ligands. Synthesis and Reactivity in Inorganic, Metal-Organic and Nano-Metal Chemistry 35 (3) (2005) 203–212.
[69] S. Afzal, A. Gul, Z. Akhter, π-Conjugated ferrocenyl Schiff base polymers: synthesis, characterization and electrical conductivity, J. Inorg. Organomet. Polym. Mater 24 (2) (2014) 321–332.
[70] M. Mazzei, et al., Synthesis of unsymmetrical methylene derivatives of benzopyran-4-ones from mannich bases, J. Heterocycl. Chem. 38 (2) (2001) 499–501.
[71] F.A. Beckford, et al., Microwave synthesis of mixed ligand diimine–thiosemicarbazone complexes of ruthenium (II): biophysical reactivity and cytotoxicity, Dalton Transactions (48) (2009) 10757–10764.
[72] J. Tomma, Synthesis of New Schiff Bases and 2, 3-Disubstituted 1, 3-Thiazolidin-4-one Derivatives Containing Benzothiazole Moiety, Ibn AL-Haitham Journal For Pure and Applied Science 24 (2) (2017).

[73] S.L. Barnholtz, et al., Syntheses and Characterization of Gold (III) Tetradentate Schiff Base Complexes. X-ray Crystal Structures of [Au (sal2pn)] Cl⊙ 2.5 H2O and [Au (sal2en)] PF6, Inorg. Chem. 40 (5) (2001) 972–976.
[74] A. Prasad, et al., Synthesis, Spectral and Electrochemical Studies of Co (II) and Zn (II) Complexes of a Novel Schiff base Derived from Pyridoxal. Synthesis and Reactivity in Inorganic, Metal-Organic, and Nano-Metal Chemistry 39 (3) (2009) 129–132.
[75] M. Shawish, H. Bashir, in: Synthesis, Characterization and Biological Studies of Nickel (II) Complexes Containing Thiosemicarbazone and Thiourea Derivatives/Hana Bashir Mohammed Shawish, University of Malaya, 2014, p. 277.
[76] R. Prabhakaran, et al., DNA binding, antioxidant, cytotoxicity (MTT, lactate dehydrogenase, NO), and cellular uptake studies of structurally different nickel (II) thiosemicarbazone complexes: synthesis, spectroscopy, electrochemistry, and X-ray crystallography, JBIC J. Biol. Inorg. Chem. 18 (2) (2013) 233–247.
[77] S.I. Mostafa, A.A. El-Asmy, M.S. El-Shahawi, Ruthenium (II) 2-hydroxybenzophenone N (4)-substituted thiosemicarbazone complexes, Transition Met. Chem. 25 (4) (2000) 470–473.
[78] R.N. Prabhu, R. Ramesh, Synthesis and structural characterization of palladium (II) thiosemicarbazone complex: application to the Buchwald–Hartwig amination reaction, Tetrahedron Lett 54 (9) (2013) 1120–1124.
[79] A.G. Bingham, et al., Synthetic, spectroscopic, and X-ray crystallographic studies on binuclear copper (II) complexes with a tridentate NNS-bonding 2-formylpyridine thiosemicarbazone ligand. The characterization of both neutral and deprotonated co-ordinated ligand structures, J. Chem. Soc., Dalton Trans. (3) (1987) 493–499.
[80] M. Mathew, G.J. Palenik, Crystal structure of bis (1-isoquinolinecarboxaldehyde thiosemicarbazonato) nickel (II) monohydrate, J. Am. Chem. Soc. 91 (23) (1969) 6310–6314.
[81] A.D. Khalaji, et al., Synthesis and Characterization of Zinc (II) Complexes with 3, 4-Dimethoxybenzaldehyde Thiosemicarbazone: the Crystal Structure of [Zn (34-MBTSC) 2Cl2], Phosphorus Sulfur. Silicon Relat. Elem. 188 (8) (2013) 1119–1126.
[82] F.M. Elmagbari, et al., Stability, solution structure and X-ray crystallography of a copper (II) diamide complex, Inorg. Chim. Acta 498 (2019) 119132.
[83] A.E. Patterson, et al., Synthesis, characterization and anticancer properties of (salicylaldiminato) platinum (II) complexes, Inorg. Chim. Acta 415 (2014) 88–94.
[84] R. Pingaew, S. Prachayasittikul, S. Ruchirawat, Synthesis, cytotoxic and antimalarial activities of benzoyl thiosemicarbazone analogs of isoquinoline and related compounds, Molecules 15 (2) (2010) 988–996.
[85] G. Lv, et al., Lipophilicity-dependent ruthenium N-heterocyclic carbene complexes as potential anticancer agents, Dalton Transac. 44 (16) (2015) 7324–7331.
[86] A.K. Bhattacharjee, J.M. Karle, Molecular electronic properties of a series of 4-quinolinecarbinolamines define antimalarial activity profile, J. Med. Chem. 39 (23) (1996) 4622–4629.
[87] F. Cheng, et al., Molecular docking and 3-D-QSAR studies on the possible antimalarial mechanism of artemisinin analogues, Biorg. Med. Chem. 10 (9) (2002) 2883–2891.
[88] M.P. Heng, et al., Mitochondria-Dependent Apoptosis Inducer: testosterone-N4-ethylthiosemicarbazonate and Its Metal Complexes with Selective Cytotoxicity Towards Human Colorectal Carcinoma Cell Line (HCT 116), Inorg. Chim. Acta (2020) 119581.
[89] M.P. Heng, K.S. Sim, K.W. Tan, Nickel and zinc complexes of testosterone N4-substituted thiosemicarbazone: selective cytotoxicity towards human colorectal carcinoma cell line HCT 116 and their cell death mechanisms, J. Inorg. Biochem. (2020) 111097.